



Article

Electrons in Quantum Dots on Helium: From Charge Qubits to Synthetic Color Centers †

Mark I. Dykman * and Johannes Pollanen

Department of Physics and Astronomy, Michigan State University, East Lansing, MI 48824, USA; pollanen@msu.edu

- * Correspondence: dykmanm@msu.edu
- [†] This paper is part of the collection in honor of P. V. E. McClintock. Peter McClintock is not only an outstanding scientist, with fundamental contributions to many areas of science, but also a remarkable human being. One of us (M.D.) has the privilege of counting Peter as a personal friend and has come to admire not only the depth of Peter's thinking, but also his kindness and warmth, his attention to not only scientific but also personal matters, and the courage to stand up for what is right.

Abstract

Electrons trapped above the surface of helium provide a means to study many-body physics free from the randomness that comes from defects in other condensed-matter systems. Localizing an electron in an electrostatic quantum dot makes its energy spectrum discrete, with controlled level spacing. The lowest two states can act as charge qubit states. In this paper, we study how the coupling to the quantum field of capillary waves on helium—known as ripplons—affects electron dynamics. As we show, the coupling can be strong. This bounds the parameter range where electron-based charge qubits can be implemented. The constraint is different from the conventional relaxation time constraint. The electron–ripplon system in a dot is similar to a color center formed by an electron defect coupled to phonons in a solid. In contrast to solids, the coupling in the electron on helium system can be varied from strong to weak. This enables a qualitatively new approach to studying color center physics. We analyze the spectroscopy of the pertinent synthetic color centers in a broad range of the coupling strength.

Keywords: charge qubits; quantum dots; electrons on helium; quantum gates; color centers; electron–phonon coupling; spectroscopy



Academic Editor: Antonio M. Scarfon

Received: 4 July 2025 Revised: 23 July 2025 Accepted: 24 July 2025 Published: 25 July 2025

Citation: Dykman, M.I.; Pollanen, J. Electrons in Quantum Dots on Helium: From Charge Qubits to Synthetic Color Centers. *Entropy* **2025**, *27*, 787. https://doi.org/10.3390/e27080787

Copyright: © 2025 by the authors. Licensee MDPI, Basel, Switzerland. This article is an open access article distributed under the terms and conditions of the Creative Commons Attribution (CC BY) license (https://creativecommons.org/licenses/by/4.0/).

1. Introduction

Studying the two-dimensional (2D) system of electrons on the surface of liquid helium is interesting in several aspects. In this system, electrons are strongly interacting with each other and are coupled to a quantum field of helium vibrations, which leads to rich and nontrivial many-body behavior. At the same time, the system is pristine, with no defects, allowing one to investigate this behavior in a controlled way, which is hard if not impossible to do in other areas of condensed-matter physics. In particular, the electron–electron interaction can be controlled by varying the electron density by several orders of magnitude, from 10^{11} cm⁻² down to 10^6 cm⁻². The strength of the coupling to the helium vibrations can also be controlled over a broad range. This coupling is determined by the electric field E_{\perp} , which presses the electrons against the helium surface and can be changed in the experiment from $\sim 10^2$ V/cm to $\sim 10^4$ V/cm.

In the overwhelming majority of experiments conducted so far, the electron system on helium was nondegenerate and the electron wave functions did not overlap. Yet, the

Entropy 2025, 27, 787 2 of 18

system is strongly correlated. The correlations are at the root of many phenomena observed in the system. These phenomena range from Wigner crystallization, which was first observed with electrons on helium [1,2], to many-electron tunneling [3,4], magnetoconductivity and cyclotron resonance [5–13], radio-frequency, microwave and piezoacoustic response [14–25], and profound nonlinear effects [26–36]. Interestingly, but not unexpectedly, the electron–electron interaction is competing with the coupling to the vibrational excitations in the helium. The latter coupling can lead to a polaronic effect [37], which can be strong, particularly in a magnetic field [38]. However, because of thermal density fluctuations in the electron liquid, an electron can be "blown away" from the polaronic well [5]. In particular, it is this effect that is behind the observed magnetoconductivity, which is very different from the conventional magnetoconductivity of other 2D electron systems [9].

In spite of the significant progress in understanding many aspects of the physics of electrons on helium, the fundamental question of the single-electron polaronic effect and its consequences remains unanswered. In this paper, we study this effect in the setting where the electron states can be well-controlled. Moreover, we show that, with electrons on helium, it becomes possible to implement, using the polaronic coupling, a "tunable synthetic color center". The importance of such an implementation follows from the fact that color centers are a prominent type of defects in solids [39]. These defects have been attracting increasing attention recently in the context of quantum measurements and quantum information [40–50]. However, in solids, the coupling between electronic transitions in color centers and phonons cannot be tuned, which limits the analysis. In contrast, this limitation does not exist for electrons on helium.

A theoretical study of the single-electron polaronic effect has been made timely by the recent progress in the experimental techniques. It is now possible to place an electron system into a high-quality-factor microwave cavity [51–53]. Quantum measurements of the cavity response enable accessing features of the electron dynamics at the single-electron level that have not been possible in the past. In parallel, precision methods have been developed for single-electron confinement in electrostatically created quantum dots on the helium surface, which can be embedded into micro-cavities [54,55]. A representative example of such a dot placed into a microwave cavity is shown in Figure 1.

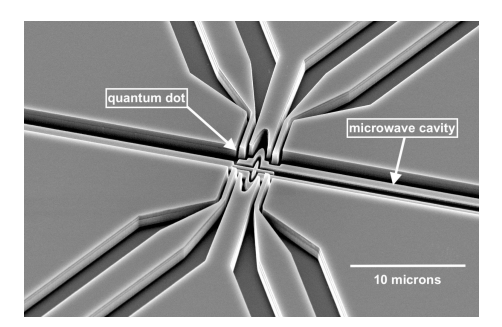


Figure 1. Electron in helium quantum dot device similar to the devices described in Ref. [54]. Trenches of order 0.5–1 μ m are dry-etched into a high-resistivity silicon to confine superfluid helium via capillary action. Electrostatic gates are defined by patterning of a pre-sputtered niobium film. They enable tuning of E_{\perp} which, in turn, enables a controlled polaronic coupling between the electron and the bosonic excitations of helium. The geometrically and electrostatically defined dot is coupled to a microwave resonator cavity to perform spectroscopy measurements of the states of the trapped electron.

In this paper, we study the response of an electron confined in a quantum dot to a resonant field that causes transitions between quantized intradot energy levels. These transitions are analogous to the transitions between the electron states of an electron Entropy 2025, 27, 787 3 of 18

localized at a defect in solid, i.e., between the states of a color center. We show that, by varying the strength of the coupling of the localized electron on helium to the helium vibrational modes, one can reproduce and explore various regimes encountered in the physics of color centers, from strong to intermediate to weak coupling.

Another motivation for this study comes from the idea of using electrons in quantum dots on helium as charge qubits [56–60]. Critical for implementing a quantum computer based on electrons on helium is understanding of the polaronic effect. In the standard terms of quantum information [61], this effect is an analog of dephasing. However, it is far more complicated and is not described by a dephasing rate. We will study how the polaronic effect is manifested in the gate operations on a charge qubit based on an electron in a quantum dot on helium. Various aspects of this effect, including the ultimate limit on the gate fidelity will be analyzed.

2. Model

We consider a geometry where electrons are floating in the x-y plane above the helium surface. They are bound to the surface by an image potential $-\Lambda/z$ for z>0, where $\Lambda=(\varepsilon-1)e^2/4(\varepsilon+1)$, with $\varepsilon\simeq 1.057$ being the helium dielectric constant; the coordinate z is counted off the surface. There is a ~ 1 eV exchange-force barrier preventing penetration into the helium. The motion of the electron normal to the surface is therefore quantized, and the spectrum is Rydberg-like, with the characteristic Bohr radius $r_B=\hbar^2/\Lambda m_e\approx 76$ Å. The spacing between the lowest and the first excited states is $\gtrsim 120$ GHz in frequency units; it largely exceeds the relevant temperatures and the energies of in-plane motion [37,62,63].

Quantum dots are created by electrodes submerged in the helium at a depth $d_{\rm dot} \simeq 0.5~\mu m$ [54,57,58]. The low-lying states of intradot electron motion are weakly non-equidistant states of two vibrational modes. We will choose the coordinates of these modes to be pointing along the x and y axes and call them x and y modes, respectively. The electron states then are the Fock states of two oscillators $|n_x,n_y\rangle$, where $n_{x,y}=0,1,2,...$ The mode eigenfrequencies Ω_x and Ω_y are controlled by the electrode potential. The Hamiltonian that describes the low-energy in-plane intradot states reads

$$H_{0} = \sum_{i=x,y} \hbar \Omega_{i} a_{i}^{\dagger} a_{i} + H_{\text{nonlin}} \qquad H_{\text{nonlin}} = \frac{1}{2} \sum_{i=x,y} \hbar V_{ii} a_{i}^{\dagger 2} a_{i}^{2} + \hbar V_{xy} a_{x}^{\dagger} a_{x} a_{y}^{\dagger} a_{y}. \tag{1}$$

Here, a_i , a_i^{\dagger} (i=x,y) are the ladder operators of the x and y modes. The parameters V_{ii} and V_{xy} describe the internal mode nonlinearities and the cross-nonlinearity, respectively. For typical quantum dots, they are small compared to $\Omega_{x,y}$. They determine the non-equidistance of the energy levels of the intradot vibrations. The smallness of the nonlinearity parameters is a consequence of the smallness of the quantum localization lengths $l_i = (\hbar/2m_e\Omega_i)^{1/2}$ (i=x,y) compared to the size of the dot; here m_e is the electron mass.

Making the dot potential asymmetric in the x and y directions allows one to make the frequencies Ω_x and Ω_y different, so that $|\Omega_x - \Omega_y| \gg |V_{xx}|, |V_{yy}|, |V_{xy}|$. Typically, for electron dots in superconducting microwave cavities, of interest are frequencies $\Omega_{x,y}$ in the range of several gigahertz. We will assume that the temperature is low, $k_BT \ll \hbar\Omega_{x,y}$, so that the electron is in the ground intradot state. Given the above estimate of the frequencies, this corresponds to temperatures $\lesssim 0.1$ –0.5 K, which are routinely used in experiments on electrons on helium.

The relevant excitations in helium are the capillary waves, ripplons, and acoustic phonons. The phonons play an important role in the electron energy relaxation. In terms of the polaronic effects, of primary interest are ripplons, which typically have low frequencies and are more strongly coupled to surface electrons [37,62]. These surface waves are

Entropy 2025, 27, 787 4 of 18

characterized by their 2D wave vector \mathbf{q} . The Hamiltonian H_{int} of the electron–ripplon coupling and the ripplon Hamiltonian H_r have the form

$$H_{\text{int}} = \sum_{\mathbf{q}} \left(V_{\mathbf{q}} e^{i\mathbf{q}\mathbf{r}} b_{\mathbf{q}} + V_{\mathbf{q}}^* e^{-i\mathbf{q}\mathbf{r}} b_{\mathbf{q}}^{\dagger} \right), \qquad H_r = \hbar \sum_{\mathbf{q}_r} \omega_q b_{\mathbf{q}}^{\dagger} b_{\mathbf{q}}, \tag{2}$$

where $\mathbf{r} = (x, y)$ is the 2D electron coordinate, $V_{\mathbf{q}}$ are the coupling parameters, ω_q is the frequency and $b_{\mathbf{q}}$ is the annihilation operator of the ripplon with wave vector \mathbf{q} . Since helium is isotropic, ω_q is independent of the direction of \mathbf{q} .

The values of V_q are obtained by projecting the overall coupling energy onto the lowest state of electron motion normal to the surface. They have the form [37]

$$V_{\bf q} = (V_{\bf q}^{({
m pol})} + eE_{\perp})(\hbar q/2\rho_{{
m He}}\omega_q S_{{
m He}})^{1/2}, \quad V_{\bf q}^{({
m pol})} \approx -(\Lambda q^2/2)[1 + \ln(qr_B/4)].$$
 (3)

Here, $V_{\bf q}^{({
m pol})}$ comes from the modulation of the image potential by surface waves. The term $\propto eE_{\perp}$ comes from the change in the electron energy in the pressing field E_{\perp} due to rising and lowering of the helium surface, and thus the electron, by surface waves; $\rho_{\rm He}$ is the helium density; and $S_{\rm He}$ is the helium surface area. We use the expression for $V_{\bf q}^{({\rm pol})}$ that applies for the variational wave function of motion normal to the surface of the form $\psi(z) \propto z \exp(-z/r_B)$. Of interest is the case where the Bohr radius r_B is small compared to typical value of q^{-1} , and we have kept the leading-order terms in qr_B ; r_B becomes a variational parameter for $E_{\perp} > 0$ (cf. [57]).

The Adiabatic Approximation

The wave numbers q of the ripplons coupled to an intradot electron are effectively limited by the reciprocal electron localization lengths l_x^{-1} , l_y^{-1} . This is seen from Equation (5) below and can be easily understood, since the effect of ripplons with wavelengths small compared to l_x , l_y is averaged out. The typical frequencies of the relevant ripplons are

$$\omega_q \lesssim \omega_{q_m}, \qquad q_m = (l_x^2 + l_y^2)^{-1/2}.$$
 (4)

They are much smaller than the electron vibration frequencies $\Omega_{x,y}$. For typical $\Omega_{x,y}/2\pi$ in the range of 3–6 GHz, we have $\omega_{q_m} \simeq 7.3 \times 10^7$ – 1.2×10^8 s $^{-1}$. As a consequence, there is no single-ripplon decay of the vibrational electron states. The main effect of the coupling to ripplons is the ripplon-induced modulation of the electron energy levels. Such modulation can be described in the adiabatic approximation. In this approximation, one keeps in the electron operator $\exp(i\mathbf{qr})$ in $H_{\rm int}$, Equation (2), only the terms that are diagonal in the intradot states, whereas the off-diagonal terms are disregarded. Respectively, the coupling Hamiltonian takes the form $H_{\rm int}^{\rm (ad)}$, where

$$H_{\text{int}}^{(\text{ad})} = \sum_{\mathbf{q}} e^{-\eta_{\mathbf{q}}} \sum_{n,m} \frac{(il_{x}q_{x})^{2n}}{n!^{2}} a_{x}^{\dagger n} a_{x}^{n} \frac{(il_{y}q_{y})^{2m}}{m!^{2}} a_{y}^{\dagger m} a_{y}^{m} (V_{\mathbf{q}}b_{\mathbf{q}} + V_{\mathbf{q}}^{*}b_{\mathbf{q}}^{\dagger}),$$

$$\eta_{\mathbf{q}} = \frac{1}{2} \sum_{i=x,y} l_{i}^{2} q_{i}^{2}.$$
(5)

Here, we used the standard expression for the components x,y of the electron displacement operator, $x=l_x(a_x^\dagger+a_x)$ and $y=l_y(a_y^\dagger+a_y)$. The nonadiabatic terms, which are disregarded in the replacement of $H_{\rm int}\to H_{\rm int}^{\rm (ad)}$, lead to small corrections to the frequencies Ω_x,Ω_y .

Entropy **2025**, 27, 787 5 of 18

The total Hamiltonian of the electron–ripplon system in a dot on helium in the adiabatic approximation is

$$H = H_0 + H_{\rm int}^{\rm (ad)} + H_r. {(6)}$$

The smallness of the characteristic ripplon frequencies ω_q compared to the frequencies $\Omega_{x,y}$ of the intradot electron excitations points to a similarity with the physics of color centers. The electron transition frequencies of color centers are often in the visible or near-infrared range [39,44,46,47], largely exceeding the phonon frequencies. The coupling to phonons in color centers is determined by the structure of the underlying defects and is often strong. However, it is not tunable in situ, whereas the coupling of an intradot electron to ripplons can be controlled by varying E_{\perp} , as seen from Equations (2) and (3). We note that the shape of the spectra of color centers is also usually analyzed in the adiabatic approximation (cf. [39,64,65]).

3. Resonant Linear Response of Intradot Electrons

Electron transitions between the intradot vibrational states have a large dipole moment $|e\mathbf{r}| \sim el_{x,y}$. Therefore, they can be comparatively strongly coupled to the intracavity microwave field (this, in fact, is what enables detecting single electrons using a microwave cavity). For temperatures $k_BT \ll \hbar\Omega_{x,y}$ the electron occupies the ground vibrational state $|n_x,n_y\rangle$ with $n_x=n_y=0$. By tuning one of the transition frequencies, for example Ω_x , close to the cavity eigenfrequency one can study the spectrum of resonant response to a microwave field associated with the transition $|0_x,0_y\rangle \rightarrow |1_x,0_y\rangle$.

The response to a weak microwave field at frequency ω is characterized by the electron conductivity. Using the Kubo formula, the diagonal component of the electron conductivity for a cavity field polarized along the x-axis can be written as

$$\sigma_{xx}(\omega) = \frac{e^2 \omega}{\hbar} \int_0^\infty dt e^{i\omega t} \langle [x(t), x(0)] \rangle, \qquad (7)$$

where $\langle \cdot \rangle$ implies thermal averaging.

The real part of σ_{xx} gives the absorption coefficient of the field. For $\omega \approx \Omega_x$ and in the case where the linewidth of the resonant peak of Re σ_{xx} is small compared to Ω_x and $|\Omega_x - \Omega_y|$, we can keep only the term $\propto \exp(-i\Omega_x t)$ in the expression for $\langle [x(t), x(0)] \rangle$. For low temperatures and $\omega \approx \Omega_x$ this gives

$$\operatorname{Re}\sigma_{xx}(\omega) \approx \frac{e^2}{2m_e}\alpha_{xx}(\omega)$$
, $\alpha_{xx}(\omega) = \operatorname{Re}\int_0^\infty dt e^{i\omega t} \langle a_x(t)a_x^{\dagger}(0)\rangle$. (8)

If there were no coupling to ripplons, we would have $\alpha_{xx}(\omega) = \pi \delta(\omega - \Omega_x)$, i.e., the cavity absorption spectrum would have the form of a δ -peak at the intradot frequency Ω_x . The electron–ripplon coupling leads to broadening of this spectroscopic peak. We note that the mode nonlinearity and the nonlinear mode coupling do not affect the spectral peak for low temperatures.

3.1. Averaging over the Ripplon States

The averaging in Equation (8) implies a trace over the electron and ripplon states with the weight $Z^{-1} \exp(-\beta H)$, where H is the full Hamiltonian of the system (see Equation (6)), $\beta = 1/k_B T$, and Z is the partition function. For typical temperatures T > 10 mK used in the experiments, the averaging should be performed assuming that the ripplons coupled to the electron are thermally excited even though the electron itself is in the ground intradot state.

Entropy 2025, 27, 787 6 of 18

The electron–ripplon coupling leads to a displacement of the ripplon equilibrium positions, i.e., deformation of the helium surface. If the electron is in the ground state, one can allow for this displacement by making a unitary transformation

$$U_g = \exp\left[\sum_{\mathbf{q}} \frac{\exp(-\eta_{\mathbf{q}})}{\hbar \omega_q} \left(V_{\mathbf{q}} b_{\mathbf{q}} - V_{\mathbf{q}}^* b_{\mathbf{q}}^{\dagger}\right)\right],\tag{9}$$

where we have taken into account the explicit form of the diagonal matrix element of the coupling Hamiltonian $H_{\rm int}^{\rm (ad)}$, Equation (5), on the electron wave function $|m_x,n_x\rangle$ with $m_x=n_x=0$.

The transformation (9) leads to a shift $b_{\bf q} \to b_{\bf q} - V_{\bf q}^* \exp(-\eta_{\bf q})/\hbar\omega_q$. When substituted into $H_{\rm int}^{\rm (ad)}$, this shift results in an adiabatic polaronic change of the frequencies and nonlinearity parameters of the electron vibrational modes. In particular, the frequency of the *x*-mode is shifted from Ω_x to $\Omega_{\rm ad}$,

$$\Omega_x \to \Omega_{\rm ad}$$
, $\Omega_{\rm ad} = \Omega_x + P_{\rm ad}$, $P_{\rm ad} = 2\sum_{\mathbf{q}} (l_x q_x)^2 |V_{\mathbf{q}}|^2 e^{-2\eta_{\mathbf{q}}} / \hbar^2 \omega_q$. (10)

The shift is quadratic in the coupling parameters and is independent of temperature.

It is convenient to calculate the correlator $\langle a_x(t)a_x^\dagger(0)\rangle$ in Equation (8) by changing to the interaction representation with the Hamiltonian \tilde{H}_0+H_r , where \tilde{H}_0 differs from H_0 in that Ω_x is replaced by $\Omega_{\rm ad}$. Then the time evolution operator becomes $U_g^\dagger \exp[-iHt]U_g=\exp[-i(\tilde{H}_0+H_r)t]\mathcal{T}_t\exp[-i\int_0^t dt_1\tilde{H}_{\rm int}^{\rm (ad)}(t_1)dt_1]$, where \mathcal{T}_t is the time ordering operator and $\tilde{H}_{\rm int}^{\rm (ad)}$ is given by Equation (5) in which the sum over m,n runs over m+n>0 (the term with m=n=0 in $H_{\rm int}^{\rm (ad)}$ has been eliminated by the canonical transformation). Tracing out the ripplonic variables in a standard way, we obtain

$$\langle a_{x}(t)a_{x}^{\dagger}(0)\rangle = e^{-i\Omega_{\text{ad}}t}\exp[-W(t)],$$

$$W(t) = \sum_{\mathbf{q}} \frac{|V_{\mathbf{q}}|^{2}}{(\hbar\omega_{q})^{2}}e^{-2\eta_{\mathbf{q}}} (l_{x}q_{x})^{4} \Big[(\bar{n}_{q}+1)\Big(1-e^{-i\omega_{q}t}\Big) + \bar{n}_{q}\Big(1-e^{i\omega_{q}t}\Big) - i\omega_{q}t \Big]$$
(11)

Here, \bar{n}_q is the thermal occupation number of a ripplon with the wave number q,

$$\bar{n}_q \equiv \bar{n}(\omega_q), \qquad \bar{n}(\omega) = [\exp(\hbar\omega/k_BT) - 1]^{-1}.$$

3.2. Radiation Emission from the Excited State

If the intradot electron is excited, it can emit radiation by going from the excited to the ground state. We will consider the radiation spectrum assuming that it is the *x*-mode that is excited and that the ripplons are in thermal equilibrium. This means that they have "adjusted" to the excited state of the mode, while the mode itself is not in thermal equilibrium; for example, it has absorbed an *x*-polarized photon, which has brought it into the first excited vibrational state, where it stays longer than it takes for the ripplons to thermalize.

The general expression for the electron emission spectrum can be found in a standard way by studying the linear response of the intradot electron to a quantized x-polarized intracavity radiation field. Near its maximum, the shape of the spectrum is given by the function

$$\tilde{a}_{xx}(\omega) = \operatorname{Re} \int_0^\infty dt e^{i\omega t} \, \overline{a_x^{\dagger}(0) a_x(t)},\tag{12}$$

where we use an overline to indicate the averaging described above.

Entropy 2025, 27, 787 7 of 18

For emission from the first excited vibrational state of the *x*-mode, a calculation similar to the one in the analysis of the absorption spectrum gives

$$\overline{a_x^{\dagger}(0)a_x(t)} = e^{-i\Omega_{\text{ad}}t} \exp\left[-W^*(t) + 2it \sum_{\mathbf{q}} \frac{|V_{\mathbf{q}}|^2}{\hbar^2 \omega_q} e^{-2\eta_{\mathbf{q}}} (l_x q_x)^4\right]$$
(13)

Measuring emission into the cavity thus provides a direct way to detect that the intradot electron was excited. Such detection is demanding, as it requires single-photon resolution. In what follows we focus on the absorption and control of electron transitions by short resonant pulses supplied to the cavity.

4. Absorption Spectrum in the Limiting Cases

Equations (8) and (11) provide an explicit general expression for the absorption spectrum of microwave radiation by an electron in a quantum dot on helium. The expression is simplified in the limiting cases of strong and weak coupling to the ripplons. The strong-coupling condition is

$$\gamma \gg \omega_{q_m}, \qquad \gamma = \hbar^{-1} \left[\sum_{\mathbf{q}} |V_{\mathbf{q}}|^2 e^{-2\eta_{\mathbf{q}}} \left(l_x q_x \right)^4 (2\bar{n}_q + 1) \right]^{1/2}.$$
 (14)

Physically, this condition means that the coupling energy, $\hbar \gamma$, is much stronger than the typical ripplonic energy $\hbar \omega_{q_m}$. When this condition holds, one can expand W(t) in Equation (11) to second order in $\omega_q t$, which gives $W(t) \approx \gamma^2 t^2/2$. Then, from Equations (8) and (11), the spectrum $\alpha_{xx}(\omega)$ has the shape of a Gaussian peak centered at $\Omega_{\rm ad}$:

$$\alpha_{xx}(\omega) \approx (\pi/2\gamma^2)^{1/2} \exp\left[-(\omega - \Omega_{ad})^2/2\gamma^2\right], \quad \gamma \gg \omega_{q_m}.$$
 (15)

The Gaussian shape of the absorption peak is familiar from the theory of strongly coupled color centers [64–66]. The characteristic width of the peak γ is linear in the coupling strength.

For a coupling that is not too strong, a very narrow zero-ripplon line emerges on the background of the broad Gaussian peak. This spectral feature is an analog of the zero-phonon lines in the spectra of color centers [39,67] and also an analog of the very narrow lines in Mössbauer spectra. The form of this line, $\alpha_{\rm zr}(\omega)$, is determined by the behavior of the function W(t) for large $\omega_{q_m}t$. In particular, the position of the line is determined by the last term in Equation (11) for W. In the approximation where we disregard processes leading to transitions between the intradot electron states, the zero-ripplon line has the form of a δ -function:

$$\alpha_{zr}(\omega) = \pi \exp(-\bar{W})\delta(\omega - \Omega_{zr}), \qquad \Omega_{zr} = \Omega_x + P_{zr},$$

$$\bar{W} = \sum_{\mathbf{q}} \frac{|V_{\mathbf{q}}|^2}{(\hbar \omega_q)^2} e^{-2\eta_{\mathbf{q}}} (l_x q_x)^4 (2\bar{n}_q + 1), \quad P_{zr} = \sum_{\mathbf{q}} \frac{|V_{\mathbf{q}}|^2}{\hbar^2 \omega_q} e^{-2\eta_{\mathbf{q}}} (l_x q_x)^2 [2 - (l_x q_x)^2]. \quad (16)$$

The zero-ripplon shift $P_{\rm zr}$ of the spectral line (16) away from the "bare" frequency Ω_x is independent of temperature. Importantly, it differs from the adiabatic line shift $P_{\rm ad}$. This means that the zero-ripplon line is shifted away from the position of the Gaussian peak (15). The factor $\exp(-\bar{W})$ is the analog of the Debye-Waller factor in the theory of x-ray and neutron scattering in solids and of the Pekar-Huang-Rhys factor in the theory of optical absorption by color centers. To the order of magnitude, $\bar{W} \sim \gamma^2/\omega_{q_m}^2$. Therefore, the zero-ripplon line (16) has an exponentially small intensity (i.e, the spectral peak has an

Entropy 2025, 27, 787 8 of 18

exponentially small area) in the limit of very strong coupling, but if the parameter \bar{W} is not too large, the line should be clearly resolved on the background of the Gaussian peak.

In the opposite limit, i.e., for weak electron–ripplon coupling, where $\bar{W} \ll 1$, the zero-ripplon line is the most intense line in the spectrum. The coupling to ripplons, besides the shift of the line from Ω_x , leads to the onset of sidebands, i.e., broad absorption bands on the higher- and lower-frequency sides of the zero-ripplon line. This is again similar to the optical spectra of impurities in solids [39,67]. From Equations (8) and (11), to the first order in \bar{W} , we have

$$\alpha_{xx}(\omega) = \alpha_{zr}(\omega) + \pi \,\mathcal{S}(\Delta\omega)[\bar{n}(\Delta\omega) + 1] + \pi \,\mathcal{S}(-\Delta\omega)\bar{n}(-\Delta\omega),$$

$$\mathcal{S}(\omega) = \sum_{\mathbf{q}} \frac{|V_{\mathbf{q}}|^2}{(\hbar\omega_q)^2} e^{-2\eta_{\mathbf{q}}} \,(l_x q_x)^4 \delta(\omega - \omega_q), \quad \Delta\omega = \omega - \Omega_{zr}.$$
(17)

This equation explicitly shows that there are two sidebands, $\mathcal{S}(\pm \Delta \omega)$. The sidebands are continuous spectra with typical width ω_{q_m} . The higher-frequency sideband, $\Delta \omega > 0$, comes from absorption where the electron and a ripplon are excited by the radiation, whereas the lower frequency sideband, $\Delta \omega < 0$, correspond to the process where the electron is excited but a ripplon is absorbed.

As seen from Equations (16) and (17), there holds the relation

$$ar{W} = \int_0^\infty d\omega \, \mathcal{S}(\omega) [2ar{n}(\omega) + 1].$$

It has a simple meaning. As seen from Equation (8), $\int_{-\infty}^{\infty} d\omega \, \alpha_{xx}(\omega) = \pi$ independent of the coupling to ripplons, whereas for weak coupling, $\int d\omega \, \alpha_{zr}(\omega) \approx \pi (1 - \bar{W})$. The reduction in the absorption in the zero-ripplon line is compensated by the sideband absorption.

Explicit Expressions in the Case of Electrons on Helium

The frequencies of ripplons coupled to the intradot electron are low. Therefore, the parameters in the expressions for the spectra should be evaluated assuming that $k_BT\gg\hbar\omega_{q_m}$. In the following, to simplify the estimates, we set $l_x=l_y$. Then, using the explicit form of the dispersion law $\omega_q=(\sigma_{\rm He}q^3/\rho_{\rm He})^{1/2}$, where $\sigma_{\rm He}$ is the surface tension, from Equation (3), we obtain the contributions \bar{W}_{E_\perp} and $\bar{W}_{\rm pol}$ of the pressing electric field and the polarization coupling to \bar{W} in the form, respectively,

$$\bar{W}_{E_{\perp}} = \frac{3e^2 E_{\perp}^2}{32\sqrt{\pi}\hbar^2} \frac{l_{\rm x}^3 \rho_{\rm He}}{\sigma_{\rm He}^2} k_B T, \qquad \bar{W}_{\rm pol} = \frac{9}{512\sqrt{\pi}} \frac{\Lambda^2 k_B T \rho_{\rm He}}{\hbar^2 \sigma_{\rm He}^2 l_x} C_{\rm pol}, \tag{18}$$

where

$$C_{\rm pol} \approx {c_{\rm pol}}^2 + 0.70 c_{\rm pol} + 0.25, \qquad c_{\rm pol} = 1 - \ln(4 l_x/r_B).$$

There is also a contribution to \bar{W} from the cross-term, which is $\propto E_{\perp}\Lambda$. We do not give an explicit expression for the corresponding term, it is smaller than the sum $\bar{W}_{E_{\perp}} + \bar{W}_{\rm pol}$. As noted earlier, r_B in the expression for $\bar{W}_{\rm pol}$ becomes a variational parameter in the presence of E_{\perp} , it is reduced from its $E_{\perp}=0$ -value. Numerically, for T=20 mK and the transition frequency $\Omega_x/2\pi=4$ GHz we have $\bar{W}_{\rm pol}\lesssim 0.05$, whereas $\bar{W}_{E_{\perp}}\lesssim 0.4$ for $E_{\perp}=100$ V/cm.

Entropy 2025, 27, 787 9 of 18

The contributions $S_{E_{\perp}}$ and S_{pol} to the sidebands from the pressing field and the polarization coupling to ripplons are, respectively,

$$S_{E_{\perp}}(\omega) = \frac{e^{2}E_{\perp}^{2}}{16\pi\hbar} \frac{l_{x}^{4}\rho_{He}^{4/3}}{\sigma_{He}^{7/3}} \exp\left[-l_{x}^{2}(\rho_{He}\omega^{2}/\sigma_{He})^{2/3}\right]\omega^{2/3}$$

$$S_{pol}(\omega) = \frac{1}{64\pi} \frac{\Lambda^{2}l_{x}^{4}\rho_{He}^{8/3}}{\hbar\sigma_{He}^{11/3}} \exp\left[-l_{x}^{2}(\rho_{He}\omega^{2}/\sigma_{He})^{2/3}\right] \tilde{C}_{pol}\omega^{10/3}$$
(19)

where $\tilde{C}_{pol} = [1 - \ln(4/q_{\omega}r_B)]^2$, with $q_{\omega} = (\rho_{He}\omega^2/\sigma_{He})^{1/3}$.

It follows from Equations (17) and (19) that the sidebands $\mathcal{S}(\pm \Delta \omega)\bar{n}(\pm \Delta \omega)$ due to the pressing field and the polarization coupling have qualitatively different shapes. Near the zero-ripplon line, the term $\propto \mathcal{S}_{pol}$ increases from zero as $|\Delta \omega|^{7/3}$ with the increasing distance from the line $\Delta \omega$, for small $|\Delta \omega|$, that is, the zero-ripplon line is well-separated from this sideband. In contrast, the sideband $\propto \mathcal{S}_{E_{\perp}}$ falls off as $|\Delta \omega|^{-1/3}$, that is, it has the form of a tail of the zero-ripplon line. This "tail" is not related to the decay of the electron states but rather to the modulation of the electron transition frequency by ripplons.

5. Single-Qubit Gates for Electrons on Helium

An important application of quantized intradot electron states is using them as charge qubit states. This is made possible by the long lifetime of the excited electron states and by the sufficiently strong nonparabolicity of the confining in-plane potential, which can be inferred already from Figure 1. The parameters $|V_{ij}|$ of the electron Hamiltonian H_{nonlin} , Equation (1), while small compared to $\Omega_{x,y}$, can be much larger than the electron decay rates and the ripplon-induced fluctuations of the electron energy levels. Therefore, radiation with frequency close to Ω_x causes interstate transitions $|0_x,0_y\rangle \to |1_x,0_y\rangle$, but does not excite transitions $|1_x,0_y\rangle \to |2_x,0_y\rangle$. The electron system can be then thought of as a quantum 2-level system, with the states $|0\rangle \equiv |0_x,0_y\rangle$ and $|1\rangle \equiv |1_x,0_y\rangle$.

Single-qubit gate operations can be performed by short resonant radiation pulses. Coupling to ripplons affects the gate fidelity, the primary effect being the modulation of the transition frequency. We will analyze some consequences of this effect by adding to the Hamiltonian (6) the term H_p that describes a microwave pulse, which has an electric field inside the dot \mathbf{E}_p that is polarized along the x-axis. The pulse has a time-dependent amplitude $E_p(t)$, and its frequency ω_p is close to Ω_x :

$$H_p = -eE_p(t)x\cos(\omega_p t + \phi_p) \approx -\hbar f_p(t)a_x e^{i\omega_p t} - \hbar f_p^*(t)a_x^{\dagger} e^{-i\omega_p t}, \tag{20}$$

Here $f_p(t) = e(l_x/2\hbar)E_p(t)\exp(i\phi_p)$, and we keep in H_p only resonant terms. We will consider the effect of a rectangular pulse of duration t_p ,

$$f_p(t) = |f_p|e^{i\phi_p}[\Theta(t) - \Theta(t - t_p)],$$

where $\Theta(t)$ is the step function, and we will use the two-state approximation. Of interest are pulses that lead to a transition $|0\rangle \to |1\rangle$. Therefore t_p is of the order of the reciprocal Rabi frequency, $t_p \sim |f_p|^{-1}$.

In this setup, the full density matrix $\hat{\rho}_{er}$ of the electron–ripplon system has four nontrivial matrix elements $\langle m_x, 0_y | \hat{\rho}_{er} | n_x, 0_y \rangle$ where m_x, n_x can take on the values 0 and 1. These matrix elements are operators with respect to ripplons. Of interest is their trace over ripplons, $\operatorname{Tr}_r \langle m_x, 0_y | \hat{\rho}_{er} | n_x, 0_y \rangle$; the ripplons are assumed to be in thermal equilibrium.

Entropy 2025, 27, 787 10 of 18

It is convenient to analyze the density matrix using the polaronic transformation

$$U_P = \exp\left[\sum_{\mathbf{q}} \frac{\exp(-\eta_{\mathbf{q}})}{\hbar \omega_q} (1 - l_x^2 q_x^2 a_x^{\dagger} a_x) (V_{\mathbf{q}} b_{\mathbf{q}} - V_{\mathbf{q}}^* b_{\mathbf{q}}^{\dagger})\right]. \tag{21}$$

After the transformation, the projection of the Hamiltonian H, Equation (6) (i.e., the Hamiltonian in the absence of the drive), on the states $|m_x, 0_y\rangle$ takes the form

$$U_P^{\dagger}HU_P \rightarrow \hbar\Omega_{zx}a_x^{\dagger}a_x + \frac{1}{2}\tilde{V}_{xx}a_x^{\dagger 2}a_x^2 + H_r.$$

Here we used that the relevant vibrational states of the *x*-mode are $|0\rangle$ and $|1\rangle$; for completeness we included the term $\propto a_x^{\dagger 2} a_x^2$, which is multiplied by the renormalized nonlinearity parameter \tilde{V}_{xx} . We note that, as a result of the transformation, the mode frequency has been changed from Ω_x to Ω_{zr} .

Further, we proceed to the rotating frame using the transformation $U_{RF} = \exp[-it(\omega_p a_x^{\dagger} a_x + \hbar^{-1} H_r)]$. As a result, we obtain a system of four operator equations for the elements of the density matrix on the electron states:

$$\rho_{mn} = \langle m | U_{RF}^{\dagger} U_{P}^{\dagger} \hat{\rho}_{er} U_{P} U_{RF} | n \rangle, \quad m, n \in \{0, 1\}.$$
 (22)

They read as follows:

$$\dot{\rho}_{00} = -i \Big(f_p^* e^{\xi^{\dagger}} \rho_{01} - f_p e^{\xi} \rho_{10} \Big), \qquad \dot{\rho}_{11} = i \Big(f_p^* e^{\xi^{\dagger}} \rho_{01} - f_p e^{\xi} \rho_{10} \Big),$$

$$\dot{\rho}_{01} = -i \Delta_p \rho_{01} - i f_p e^{\xi} (\rho_{00} - \rho_{11}), \quad \rho_{10} = (\rho_{01})^{\dagger}, \tag{23}$$

where

$$\xi \equiv \xi(t) = -\sum_{\mathbf{q}} \frac{\exp(-\eta_{\mathbf{q}})}{\hbar \omega_{q}} l_{x}^{2} q_{x}^{2} \left(V_{\mathbf{q}} b_{\mathbf{q}} e^{-i\omega_{q}t} - V_{\mathbf{q}}^{*} b_{\mathbf{q}}^{\dagger} e^{i\omega_{q}t} \right), \quad \Delta_{p} = \omega_{p} - \Omega_{zr}. \quad (24)$$

We used the fact that

$$U_P^{\dagger}H_pU_P = -\hbar f_p(t)a_x e^{i\omega_p t} \exp[\xi(0)] + \text{H.c.}$$

The parameter Δ_p in Equation (23) is the detuning of the drive frequency from the frequency of the zero-ripplon line of the electron in the quantum dot. We assume that $|\Delta_p| \ll \omega_p$. The operator $\xi(t)$ is anti-Hermitian, $\xi^{\dagger}(t) = -\xi(t)$, and one can check that $\langle \xi(t)\xi^{\dagger}(t)\rangle = \bar{W}$.

5.1. The Effects of Quantum and Classical Ripplon-Induced Fluctuations

Of interest to us are Rabi oscillations of the electron in the presence of coupling to ripplons, i.e., the evolution of the populations of the states $|0\rangle$ and $|1\rangle$. These populations are given by the traces of ${\rm Tr}_r\rho_{00}$ and ${\rm Tr}_r\rho_{11}$ over ripplonic states. From Equation (23), it is seen that the time evolution of ρ_{mn} is characterized by the frequency $\sim |f_p|$. Therefore, ripplons with frequencies $\omega_q\gg |f_p|$ are averaged out. Typically, $|f_p|\ll k_BT/\hbar$. Therefore, it is a good approximation to assume that quantum fluctuations of the ripplonic field as a whole are averaged out; here, we take into account that the coupling to low-frequency

Entropy 2025, 27, 787 11 of 18

quantum fluctuations of this field is weak (cf. Equation (19)). Then, in Equation (23) we can replace

$$f_p(t) e^{\xi(t)} \to \widetilde{f}_p(t), \qquad \widetilde{f}_p(t) = \overline{f}_p \exp[\xi_T(t)],$$

$$\overline{f}_p = |f_p| e^{i\phi_p} \exp[-\overline{W}_q], \quad \overline{W}_q = \frac{1}{2} \sum_{\mathbf{q}} \frac{|V_{\mathbf{q}}|^2}{(\hbar \omega_q)^2} e^{-2\eta_{\mathbf{q}}} (l_x q_x)^4. \tag{25}$$

Here, \bar{W}_q is half the contribution to the Debye-Waller factor \bar{W} at T=0 (cf. Equation (16)).

The term $\xi_T(t)$ accounts for the coupling to thermal ripplons. Typically, their frequencies ω_q satisfy the condition $\omega_q \ll k_B T/\hbar$. From Equation (24), the correlation function of $\xi_T(t)$ is obtained from the correlation function of $\xi(t)$ by keeping the terms $\propto \bar{n}_q \approx k_B T/\hbar \omega_q$,

$$\Xi(t-t') = \langle \xi_T(t)\xi_T^{\dagger}(t')\rangle = 2k_B T \sum_{\mathbf{q}} \frac{|V_{\mathbf{q}}|^2}{(\hbar\omega_q)^3} e^{-2\eta_{\mathbf{q}}} \left(l_x q_x\right)^4 \cos[\omega_q(t-t')], \tag{26}$$

whereas the commutator $\langle [\xi_T(t), \xi_T^{\dagger}(t')] \rangle$ is smaller than $\Xi(t-t')$ by a factor $\sim \hbar \omega_{q_m}/k_BT$. Therefore $\xi_T(t) = -\xi_T^{\dagger}(t)$ is essentially a classical zero-mean Gaussian noise with the correlator $\Xi(t)$. This noise affects Rabi oscillations. Tracing over ripplons becomes equivalent to statistical averaging over the realizations of the noise $\xi_T(t)$.

We note that the time-averaging used to obtain \bar{W}_q is not limited to the coupling to ripplons. However, the approximation $\omega_q \ll k_B T/\hbar$ is specific for ripplons, given the low temperatures used in quantum computing systems. We also note a simple relation between the noise correlator $\Xi(t)$ and the sideband spectral density $\mathcal{S}(\omega)$,

$$\Xi(t) = \int_0^{\omega_T} d\omega \, \frac{2k_B T}{\hbar \omega} \, \mathcal{S}(\omega) \cos \omega t,$$

where the cutoff ω_T is $\lesssim k_B T/\hbar$; as explained above, for electrons on helium one can set $\omega_T \to \infty$, given the exponential falloff of $\mathcal{S}(\omega)$ that typically occurs already for $\omega \ll k_B T/\hbar$.

5.1.1. Nonergodic Response

The problem of Rabi oscillations can be solved in several limiting cases. One of them is the case of comparatively large drive and, respectively, short pulses t_p . If the typical ripplon frequency ω_{q_m} is small compared to t_p^{-1} , i.e., the correlation time of the noise ξ_T is large compared to t_p , one can replace $\xi_T(t)$ in Equation (25) for $\widetilde{f}_p(t)$ with $\xi_T(0)$, so that $\widetilde{f}_p(t)$ becomes time-independent. Then Equation (23) becomes a standard equation for Rabi oscillations with a time-independent drive. The noise determines the static random phase of the drive. If the electron is initially in the ground state and the Rabi frequency $R_{\text{nonergodic}}$ is extracted from the occupation of the excited state in response to a pulse, from Equation (23) we find

$$R_{\text{nonergodic}} = \left\{ \Delta_p^2 + 4 | \overline{f_p}|^2 \right\}^{1/2}.$$

Unexpectedly, the Rabi frequency measured this way is independent of the noise.

However, the off-diagonal matrix elements $\rho_{01} = \rho_{10}^*$ depend on a particular realization of the noise. If the noise is so slow that several measurements of ρ_{01} can be repeated for the same value of ξ_T to average over the quantum measurements outcomes, the result will be nonergodic. It will depend on a particular value of ξ_T and will not include averaging over ξ_T (cf. [68]). In other words, the values of ρ_{01} will be different in different series of such measurements.

For an electron in a quantum dot on helium, if the electron transition frequency is $\Omega_x/2\pi \sim 4$ GHz, the correlation time of the noise from thermal ripplons is

Entropy 2025, 27, 787 12 of 18

 $2\pi/\omega_{q_m}\lesssim 10^{-7}$ s. Therefore, even with $\sim\!10$ ns-long control and measurement pulses, it will be difficult to accumulate enough measurements for the same configuration of the ripplonic field. More realistic nonergodic measurements would help revealing noise from nonthermal fluctuations of the helium surface and from the varying configuration of stray electrons in the cavity, as such electrons are often inadvertently deposited along with the electrons that go into the quantum dots. The measurements would provide an important insight into the nature of the fluctuations, including density and the dynamics of stray electrons.

If the pulses are short in the sense that $\omega_{q_m}t_p\ll 1$, but the noise from thermal ripplons ξ_T varies from measurement to measurement, one can still assume that ξ_T is constant during a pulse. In this case measurement outcomes will have to be averaged over the realizations of ξ_T . For example, if the electron is in the ground state at t=0 and $\Delta_p=0$, we have from Equation (23)

$$\rho_{01}(t) = -i\frac{f_p}{2|f_p|} \exp[\xi_T(0)] \sin(2|\overline{f_p}|t).$$

The results of uncorrelated measurements of ρ_{01} given by this expression have to be averaged over the Gaussian distribution of the thermal noise $\xi_T(0)$.

5.1.2. Response to a Resonant Pulse for Strong Electron–Ripplon Coupling

More accessible are measurements where ω_{q_m} is comparable or larger than t_p^{-1} . In this case, the variation of $\xi_T(t)$ during a pulse has to be taken into account. We will study the response to a resonant pulse, assuming that at t=0 the electron is in the ground state. Tracing over ripplons will be replaced by averaging over the classical noise $\xi_T(t)$. From Equation (23) we obtain an equation for the difference in the state populations $\mathcal{N}(t) = \rho_{00}(t) - \rho_{11}(t)$, which reads

$$\frac{d}{dt}\mathcal{N}(t) = -2|\overline{f_p}|^2 \int_0^t dt' \exp\left[-i\Delta_p(t-t') - \xi_T(t) + \xi_T(t')\right] \mathcal{N}(t') + \text{c.c.}.$$
 (27)

For strong coupling to ripplons, $\bar{W}\gg 1$, the mean value of the random factor in Equation (27),

$$\langle \exp[-\xi_T(t) + \xi_T(t')] \rangle = \exp[-\Xi(0) + \Xi(t - t')] \approx \exp[-\gamma^2(t - t')^2/2],$$
 (28)

rapidly falls off with the increasing t-t'. In the above expression we used Equation (14) for the parameter γ , in which we replaced $2\bar{n}_q+1$ with $2k_BT/\hbar\omega_q$. We also used that $\gamma\gg\omega_{q_m}$ for strong coupling, and therefore $\omega_q|t-t'|\ll 1$ for $|t-t'|\lesssim 1/\gamma$.

If $|\overline{f_p}| \ll \gamma$, it is seen from Equation (27) that $\mathcal{N}(t)$ slowly varies on the time scale γ^{-1} . Then in this equation one can replace $\mathcal{N}(t')$ in the integrand with $\mathcal{N}(t)$, which gives

$$\langle \mathcal{N}(t) \rangle = \langle \mathcal{N}(0) \rangle \exp(-\Gamma_{\rm sc} t), \quad \Gamma_{\rm sc} = \frac{\sqrt{8\pi}}{\gamma} |\overline{f_p}|^2 \exp(-\Delta_p^2/2\gamma^2).$$
 (29)

As seen from this equation, rather than experiencing Rabi oscillations, the difference in the state populations exponentially decays in time, that is, the populations of the state $|0\rangle$ and $|1\rangle$ approach each other. The decay rate in the strong-coupling limit is $\Gamma_{\rm sc} \ll |\overline{f_p}|$. This rate falls off with the increasing strength of the coupling to ripplons, which determines γ , and in particular with the increasing temperature. It is quadratic in the amplitude of the radiation pulse α $|\overline{f_p}|$.

Entropy 2025, 27, 787 13 of 18

The condition $\Gamma_{\rm sc} \ll \gamma$, which underlies replacing $\mathcal{N}(t')$ with $\mathcal{N}(t)$ in Equation (27), is met "automatically", since $|\overline{f_p}| \ll \gamma$. The corresponding inequalities also justify the next step, in which $\mathcal{N}(t)$ is replaced with $\langle \mathcal{N}(t) \rangle$.

Equation (29) shows that, practically, one cannot perform coherent gate operations on a charge qubit if the coupling of the underlying electron to ripplons is strong, at least unless the microwave field is so strong that $f_p \gg \gamma$ and the operations are carried out over time smaller than γ^{-1} . The constraint is not related to the lifetime of the excited electron state. It also may not be directly mapped on qubit decoherence described by the standard T_2 -type process.

5.1.3. Response to a Resonant Pulse for Weak Coupling to Ripplons

We now consider the effect of a radiation pulse in the case of weak electron–ripplon coupling. It is important to make sure that the divergence of $\mathcal{S}(\omega)/\omega$ for $\omega \to 0$ does not make it impossible to perform reliable single-qubit gates. Moreover, it is necessary to estimate the gate error related to the coupling to ripplons.

We will again assume that initially (t=0) the qubit is in the ground state, $\langle \mathcal{N}(0) \rangle = 1$, and that $\Delta_p = 0$, i.e., the pulse frequency ω_p is equal to the zero-ripplon transition frequency $\Omega_{\rm zr}$. We will find the lowest-order in ξ_T correction to \mathcal{N} . To do it, we rewrite Equation (27) in the form

$$\frac{d^2}{dt^2}\mathcal{N} + 4|\overline{f_p}|^2\mathcal{N} = 2|\overline{f_p}|^2\frac{d\xi_T(t)}{dt}\int_0^t dt' \mathcal{N}(t')\exp[-\xi_T(t) + \xi_T(t')] + \text{c.c.}$$

The zeroth-order solution $\mathcal{N}^{(0)}(t)$ of this equation describes Rabi oscillations,

$$\mathcal{N}^{(0)}(t) = \cos(2|\overline{f_p}|t). \tag{30}$$

The correction to $\mathcal{N}(t)$ of the lowest order in ξ_T has the form

$$\mathcal{N}^{(1)}(t) = \frac{2|\overline{f_p}|k_B T}{\hbar} \int_0^\infty d\omega \frac{\omega \,\mathcal{S}(\omega)}{(\omega^2 - 4|\overline{f_p}|^2)^2} \times \left\{ 4|\overline{f_p}|[\cos(\omega t) - \cos(2|\overline{f_p}|t)] + (\omega^2 - 4|\overline{f_p}|^2)t \,\sin(2|\overline{f_p}|t) \right\}$$
(31)

This equation shows that the correction to the Rabi-oscillation term (30) increases with the increasing temperature. It is seen that the major contribution to $\mathcal{N}^{(1)}(t)$ comes from the range of frequencies of the sideband spectrum $\mathcal{S}(\omega)$ where $\omega \sim 2|\overline{f_p}|$, i.e., from the range where the noise "resonates" with the Rabi oscillations; the contributions from the low- and high-frequency parts of $\mathcal{S}(\omega)$ are suppressed. Interestingly, the function $\mathcal{N}^{(1)}(t)$ displays oscillations at the Rabi frequency with an amplitude that increases with time.

Overall, Equation (31) shows that the correction to the qubit dynamics is small for weak coupling. However, the form of the correction is somewhat unexpected. The explicit expression for $\mathcal{N}^{(1)}(t)$ makes it possible to find an optimal value of the Rabi frequency $2|\overline{f_p}|$ for a desired gate operation. In particular, a contribution to $\mathcal{N}^{(1)}(t)$ from the pressing field for a π pulse, $2|\overline{f_p}|t=\pi$, for the typical parameter values $E_{\perp}=100$ V/cm and T=20 mK is well approximated by the expression

$$\mathcal{N}_{E_{\perp}}^{(1)} pprox rac{e^2 E_{\perp}^2 k_B T l_x^4}{32 \hbar^2} rac{
ho_{\mathrm{He}}^{4/3}}{\sigma_{\mathrm{He}}^{7/3}} (2 |\overline{f_p}|/\pi)^{2/3},$$

which gives $\sim 8 \times 10^{-3}$ for the pulse duration $\pi/2|\overline{f_p}|=10^{-6}$ s. The gate error can be reduced using longer pulses, lower temperatures, and weaker pressing fields.

Entropy 2025, 27, 787 14 of 18

Since the typical sideband frequency $\omega_{q_m}/2\pi$ is ~20–30 MHz, it is straightforward to separate the zero-ripplon line from the sidebands if the quality factor of the cavity is >10³. This requirement is easily met in superconducting cavities. We note also that the direct Coulomb interaction between electrons in neighboring quantum dots provides a natural way of implementing two-qubit gates, as was envisioned early on [56,57]. The relevant parameter is the Coulomb frequency $\omega_C = [(d^2V_{\rm id}/dr^2)/m_e]^{1/2}$, where $V_{\rm id}$ is the coupling potential. This potential may be modified from the direct Coulomb potential by the screening from the electrodes. If the screening is inessential, $\omega_C/2\pi \approx 0.23$ GHz for an interdot distance of 5 µm. This frequency should be small compared to the difference in the eigenfrequencies Ω_x in different dots. A gate operation can be performed by tuning the eigenfrequencies in different dots in resonance. Since there are no two-level systems in the system, the tuning is protected from resonance-related errors typically associated with such systems.

6. Discussion

The results of this paper show that electrons in quantum dots on helium surface provide an extremely rich system to explore. Their energy spectrum is discrete and can be controlled electrostatically. When the system is embedded into a microwave cavity, one can observe resonant transitions between the energy levels. This underlies using the electron states as charge qubit states. However, even though the system is free from defects, the electron coupling to the quantum field of ripplons may pose an obstacle to implementing charge qubits. The physics here is different from the conventional analysis of the processes that lead to electron relaxation. It is rather related to the physics encountered in the studies of color centers in solids.

The effect of the coupling on gate operations can be reduced to an effective Debye-Waller factor, which is due to quantum fluctuations and decreases the amplitude of the driving field, and a classical noise that modulates this amplitude. Such description is possible because, for typical parameters of quantum dots on helium, the frequencies of the ripplons coupled to an electron are small compared to k_BT/\hbar . The slowness of the ripplons may lead to nontrivial measurement outcomes, particularly if the measurements are fast.

Further insight can be gained using the explicit expression for the characteristic dimensionless parameter of the electron–ripplon coupling that we provide. If this parameter is large, it means that the coupling is strong. In this regime, practically, one cannot perform coherent gate operations on an electron charge qubit. The coupling depends on the electron localization length in the dot, the temperature, and most importantly, the field E_{\perp} that presses the electrons against the helium surface. This field is necessary to prevent "evaporation" of the electrons from the surface. As we show, for the coupling parameter to be small, E_{\perp} must be comparatively small itself, $\lesssim 100$ V/cm. For weak coupling, the error of single-qubit gate operations can be small; it can be estimated using the explicit expressions provided in the paper.

The possibility to vary the coupling to ripplons from weak to strong opens a unique way of studying physics of color centers formed by electronic defects in solids. The electron-ripplon coupling mimics the electron-phonon coupling in color centers in solids. This is despite the energy scales being vastly different. The transitions frequencies of color centers are in the range of a few electron-volts. For F-centers in alkali halide crystals the typical phonon energies are in the range of 0.02–0.03 eV [39], and for NV^- centers in diamond they are in the range of 0.1 eV, whereas for the ripplons coupled to an intradot electron they are typically $\sim 10^{-7}$ eV. At the same time, the dimensionless coupling parameter \bar{W} , the Pekar-Huang-Rhys factor can reach 20–30 and more for F-centers [69,70], and it is ~ 3.5 –4 for an NV^- center [71]; these numbers are easy to emulate with electrons in quantum dots

Entropy 2025, 27, 787 15 of 18

on helium. Impurity atoms in liquid helium also often have broad spectral lines [72], as they form bubbles and are thus strongly coupled to helium vibrations. Bubbles are also formed by single electrons in helium. An electron confined to a bubble seems to be the closest system to an electron in a quantum dot, but a major difference is that the bubbles are small, with radius ~ 17 Å. Therefore the characteristic excitation energies in the bubbles are much higher, ~ 0.1 eV, and the frequencies of the vibrational modes of helium are $\sim 5 \times 10^{-5}$ eV; the coupling to these modes is strong, leading to the linewidth $\sim 10^{-3}$ eV for T=0 [73].

Spectral lines of color centers as well as impurities and electrons confined to bubbles in helium have a complicated structure. The change in the structure with the varying coupling parameters could not be explored. For electrons on helium, the variability of the coupling is enabled by E_{\perp} . Our results show how the electron absorption spectrum changes with decreasing E_{\perp} from a comparatively broad Gaussian peak with a superposed weak zero-ripplon line, for large E_{\perp} , to a strong narrow zero-ripplon peak, for small E_{\perp} , with sidebands that have a characteristic form.

The linear and nonlinear response of a localized electron to a resonant electromagnetic field and the change in this response with the varying control parameters open a path to a better understanding of the electron coupling to a quantized field of helium vibrations, including the features of the coupling in confined geometries. It also provides a means to study the overall structure of the electron motional states in a quantum dot on the helium surface. In a broader context, the system offers a controlled platform for studying the effects of electron coupling to a bosonic field.

Author Contributions: The authors have contributed equally. All authors have read and agreed to the published version of the manuscript.

Funding: This work was supported in part by the National Science Foundation via grant number DMR-2003815. MID acknowledges partial support from the Google Faculty Award and from the Gordon and Betty Moore Foundation Award No. GBMF12214. JP acknowledges partial support from the Cowen Family Endowment at MSU.

Data Availability Statement: Data is contained within the article.

Conflicts of Interest: MID declares no competing interests. JP is a co-founder and CSO of EeroQ Corp.

References

- 1. Grimes, C.C.; Adams, G. Evidence for a Liquid-to-Crystal Phase-Transition in a Classical, 2-Dimensional Sheet of Electrons. *Phys. Rev. Lett.* **1979**, 42, 795–798. [CrossRef]
- 2. Fisher, D.S.; Halperin, B.I.; Platzman, P.M. Phonon-Ripplon Coupling and the 2-Dimensional Electron Solid on a Liquid-Helium Surface. *Phys. Rev. Lett.* **1979**, 42, 798–801. [CrossRef]
- 3. Menna, L.; Yucel, S.; Andrei, E.Y. Giant Magnetic Suppression of Tunneling out of a 2d Electron-System. *Phys. Rev. Lett.* **1993**, 70, 2154–2157. [CrossRef] [PubMed]
- 4. Dykman, M.I.; Sharpee, T.; Platzman, P.M. Enhancement of Tunneling from a Correlated 2D Electron System by a Many-Electron Mossbauer-Type Recoil in a Magnetic Field. *Phys. Rev. Lett.* **2001**, *86*, 2408–2411. [CrossRef] [PubMed]
- 5. Dykman, M.I.; Khazan, L.S. Effect of the Interaction between Nondegenerate Electrons Localized in a Thin Surface Layer on the Cyclotron Resonance and on the Magnetoconductance. *J. Exp. Theor. Phys.* **1979**, *50*, 747.
- 6. Edelman, V.S. Investigation of the Resonance Properties of Electrons Localized above Liquid 3he and 4he. *J. Exp. Theor. Phys.* **1979**, *50*, 338.
- 7. Iye, Y. Mobility of Electrons in the Surface-State of Liquid-Helium. J. Low Temp. Phys. 1980, 40, 441–451. [CrossRef]
- 8. Wilen, L.; Giannetta, R. Cyclotron Resonance of the Two-Dimensional Electron Crystal. *Phys. Rev. Lett.* **1988**, *60*, 231–234. [CrossRef]
- 9. Dykman, M.I.; Lea, M.J.; Fozooni, P.; Frost, J. Magnetoresistance in 2D Electrons on Liquid-Helium—Many-Electron versus Single-Electron Kinetics. *Phys. Rev. Lett.* **1993**, *70*, 3975–3978. [CrossRef]
- 10. Lea, M.J.; Fozooni, P.; Richardson, P.J.; Blackburn, A. Direct Observation of Many-Electron Magnetoconductivity in a Nondegenerate 2d Electron Liquid. *Phys. Rev. Lett.* **1994**, *73*, 1142–1145. [CrossRef]

Entropy 2025, 27, 787 16 of 18

11. Monarkha, Y.P.; Ito, S.; Shirahama, K.; Kono, K. Inelastic Quantum Magnetotransport in a Highly Correlated Two-Dimensional Electron Liquid. *Phys. Rev. Lett.* **1997**, *78*, 2445–2448. [CrossRef]

- 12. Mistura, G.; Tress, O.; Teske, E.; Shikin, V.; Wyder, P.; Leiderer, P. Microwave Study of Surface Electrons on Helium Films in a Magnetic Field. *J. Low Temp. Phys.* **1998**, 110, 243–248. [CrossRef]
- 13. Klier, J.; Wurl, A.; Leiderer, P.; Mistura, G.; Shikin, V. Cyclotron Resonance for Two-Dimensional Electrons on Thin Helium Films. *Phys. Rev. B* **2002**, *65*, 165428. [CrossRef]
- 14. ANDREI, E.Y. 2d-Electron Systems Viewed through an Rf Spectrometer. Physica B 1994, 197, 335–339. [CrossRef]
- 15. Konstantinov, D.; Dykman, M.I.; Lea, M.J.; Monarkha, Y.; Kono, K. Resonant Correlation-Induced Optical Bistability in an Electron System on Liquid Helium. *Phys. Rev. Lett.* **2009**, *103*, 096801. [CrossRef]
- 16. Konstantinov, D.; Kono, K. Photon-Induced Vanishing of Magnetoconductance in 2D Electrons on Liquid Helium. *Phys. Rev. Lett.* **2010**, *105*, 226801. [CrossRef]
- 17. Konstantinov, D.; Monarkha, Y.; Kono, K. Effect of Coulomb Interaction on Microwave-Induced Magnetoconductivity Oscillations of Surface Electrons on Liquid Helium. *Phys. Rev. Lett.* **2013**, *111*, 266802. [CrossRef]
- 18. Yunusova, K.M.; Konstantinov, D.; Bouchiat, H.; Chepelianskii, A.D. Coupling between Rydberg States and Landau Levels of Electrons Trapped on Liquid Helium. *Phys. Rev. Lett.* **2019**, 122, 176802. [CrossRef]
- 19. Chepelianskii, A.D.; Konstantinov, D.; Dykman, M.I. Many-Electron System on Helium and Color Center Spectroscopy. *Phys. Rev. Lett.* **2021**, *127*, 016801. [CrossRef]
- 20. Kawakami, E.; Elarabi, A.; Konstantinov, D. Relaxation of the Excited Rydberg States of Surface Electrons on Liquid Helium. *Phys. Rev. Lett.* **2021**, *126*, 106802. [CrossRef]
- 21. Byeon, H.; Nasyedkin, K.; Lane, J.R.; Beysengulov, N.R.; Zhang, L.; Loloee, R.; Pollanen, J. Piezoacoustics for Precision Control of Electrons Floating on Helium. *Nat. Commun.* **2021**, *12*, 4150. [CrossRef]
- 22. Li, Y.; He, S.; Zhang, M.; Wei, L. Quantum Computation with Electrons Trapped on Liquid Helium by Using the Centimeter-Wave Manipulating Techniques. *Quantum Inf. Process.* **2024**, 23, 294. [CrossRef]
- 23. He, M.; Cheng, Z. Transfer of electrons floating on helium by surface acoustic waves. *Sci. China Phys. Mech. Astron.* **2025**, 68, 277011.
- 24. Jennings, A.; Grytsenko, I.; Tian, Y.; Rybalko, O.; Wang, J.; Barabash, J.; Kawakami, E. Probing the Quantum Capacitance of Rydberg Transitions of Surface Electrons on Liquid Helium via Microwave Frequency Modulation. *arXiv* 2025, arXiv:2504.09890. [CrossRef]
- 25. Mikolas, C.A.; Beysengulov, N.R.; Schleusner, A.J.; Rees, D.G.; Undershute, C.; Pollanen, J. Plasmon mode engineering with electrons on helium. *Nat. Commun.* **2025**, *16*, 4959. [CrossRef]
- 26. Kristensen, A.; Djerfi, K.; Fozooni, P.; Lea, M.J.; Richardson, P.J.; Santrich-Badal, A.; Blackburn, A.; van der Heijden, R.W. Hall-Velocity Limited Magnetoconductivity in a Classical Two-Dimensional Wigner Crystal. *Phys. Rev. Lett.* **1996**, 77, 1350–1353. [CrossRef]
- 27. Dykman, M.I.; Rubo, Y.G. Bragg-Cherenkov Scattering and Nonlinear Conductivity of a Two-Dimensional Wigner Crystal. *Phys. Rev. Lett.* **1997**, *78*, 4813–4816. [CrossRef]
- 28. Vinen, W.F. Non-Linear Electrical Conductivity and Sliding in a Two-Dimensional Electron Crystal on Liquid Helium. *J. Phys. Condens. Matter* **1999**, *11*, 9709. [CrossRef]
- 29. Glasson, P.; Dotsenko, V.; Fozooni, P.; Lea, M.J.; Bailey, W.; Papageorgiou, G.; Andresen, S.E.; Kristensen, A. Observation of Dynamical Ordering in a Confined Wigner Crystal. *Phys. Rev. Lett.* **2001**, *87*, 176802. [CrossRef]
- 30. Collin, E.; Bailey, W.; Fozooni, P.; Frayne, P.G.; Glasson, P.; Harrabi, K.; Lea, M.J.; Papageorgiou, G. Microwave Saturation of the Rydberg States of Electrons on Helium. *Phys. Rev. Lett.* **2002**, *89*, 245301. [CrossRef]
- 31. Ikegami, H.; Akimoto, H.; Kono, K. Nonlinear Transport of the Wigner Solid on Superfluid He-4 in a Channel Geometry. *Phys. Rev. Lett.* **2009**, *102*, 046807. [CrossRef] [PubMed]
- 32. Rees, D.G.; Kuroda, I.; Marrache-Kikuchi, C.A.; Hofer, M.; Leiderer, P.; Kono, K. Transport Measurements of Strongly Correlated Electrons on Helium in a Classical Point-Contact Device. *J. Low Temp. Phys.* **2012**, *166*, 107–124. [CrossRef]
- 33. Chepelianskii, A.D.; Watanabe, M.; Nasyedkin, K.; Kono, K.; Konstantinov, D. An Incompressible State of a Photo-Excited Electron Gas. *Nat. Commun.* **2015**, *6*, 7210. [CrossRef] [PubMed]
- 34. Rees, D.G.; Beysengulov, N.R.; Lin, J.J.; Kono, K. Stick-Slip Motion of the Wigner Solid on Liquid Helium. *Phys. Rev. Lett.* **2016**, 116, 206801. [CrossRef]
- 35. Rees, D.G.; Beysengulov, N.R.; Teranishi, Y.; Tsao, C.S.; Yeh, S.S.; Chiu, S.P.; Lin, Y.H.; Tayurskii, D.A.; Lin, J.J.; Kono, K. Structural Order and Melting of a Quasi-One-Dimensional Electron System. *Phys. Rev. B* **2016**, *94*, 045139. [CrossRef]
- 36. Siddiq, H.; Nasyedkin, K.; Kono, K.; Zmeev, D.E.; McClintock, P.V.E.; Pashkin, Y.A.; Stefanovska, A. Visualization of Oscillatory Electron Dynamics on the Surface of Liquid Helium. *Phys. Rev. B* **2023**, *107*, 104501. [CrossRef]
- 37. Shikin, V.; Monarkha, Y.P. On the Interaction of Surface Electrons in Liquid Helium with Oscillations of the Vapor-Liquid Interface. *J. Low Temp. Phys.* **1974**, *16*, 193–208. [CrossRef]

Entropy 2025, 27, 787 17 of 18

38. Dykman, M.I. Theory of Cyclotron Resonance of Two-Dimensional Electrons Interacting with Surface and Volume Phonons. *Phys. Status Solidi (b)* **1978**, *88*, 463. [CrossRef]

- 39. Stoneham, A.M. Theory of Defects in Solids; Oxford University Press: Oxford, UK, 2001.
- 40. Maze, J.R.; Stanwix, P.L.; Hodges, J.S.; Hong, S.; Taylor, J.M.; Cappellaro, P.; Jiang, L.; Dutt, M.V.G.; Togan, E.; Zibrov, A.S.; et al. Nanoscale magnetic sensing with an individual electronic spin in diamond. *Nature* **2008**, 455, 644–647. [CrossRef]
- 41. Grinolds, M.S.; Hong, S.; Maletinsky, P.; Luan, L.; Lukin, M.D.; Walsworth, R.L.; Yacoby, A. Nanoscale Magnetic Imaging of a Single Electron Spin under Ambient Conditions. *Nat. Phys.* **2013**, *9*, 215–219. [CrossRef]
- 42. Myers, B.A.; Das, A.; Dartiailh, M.C.; Ohno, K.; Awschalom, D.D.; Bleszynski Jayich, A.C. Probing Surface Noise with Depth-Calibrated Spins in Diamond. *Phys. Rev. Lett.* **2014**, *113*, 027602. [CrossRef]
- 43. Becker, J.N.; Pingault, B.; Groß, D.; Gündoğan, M.; Kukharchyk, N.; Markham, M.; Edmonds, A.; Atatüre, M.; Bushev, P.; Becher, C. All-Optical Control of the Silicon-Vacancy Spin in Diamond at Millikelvin Temperatures. *Phys. Rev. Lett.* **2018**, *120*, 053603. [CrossRef] [PubMed]
- 44. Awschalom, D.D.; Hanson, R.; Wrachtrup, J.; Zhou, B.B. Quantum Technologies with Optically Interfaced Solid-State Spins. *Nat. Photonics* **2018**, *12*, 516–527. [CrossRef]
- 45. Chen, Y.C.; Griffiths, B.; Weng, L.; Nicley, S.S.; Ishmael, S.N.; Lekhai, Y.; Johnson, S.; Stephen, C.J.; Green, B.L.; Morley, G.W.; et al. Laser writing of individual nitrogen-vacancy defects in diamond with near-unity yield. *Optica* **2019**, *6*, 662–667. [CrossRef]
- 46. Barry, J.F.; Schloss, J.M.; Bauch, E.; Turner, M.J.; Hart, C.A.; Pham, L.M.; Walsworth, R.L. Sensitivity Optimization for NV-Diamond Magnetometry. *Rev. Mod. Phys.* **2020**, 92, 015004. [CrossRef]
- 47. Bhaskar, M.K.; Riedinger, R.; Machielse, B.; Levonian, D.S.; Nguyen, C.T.; Knall, E.N.; Park, H.; Englund, D.; Lončar, M.; Sukachev, D.D.; et al. Experimental Demonstration of Memory-Enhanced Quantum Communication. *Nature* **2020**, *580*, 60–64. [CrossRef]
- 48. Huxter, W.S.; Palm, M.L.; Davis, M.L.; Welter, P.; Lambert, C.H.; Trassin, M.; Degen, C.L. Scanning Gradiometry with a Single Spin Quantum Magnetometer. *Nat. Commun.* **2022**, *13*, 3761. [CrossRef]
- 49. Xu, S.; Liu, M.; Xie, T.; Zhao, Z.; Shi, Q.; Yu, P.; Duan, C.K.; Shi, F.; Du, J. High-Precision Measurements and First-Principles Explanation of the Temperature-Dependent ¹³C and ¹⁴N Hyperfine Interactions of Single NV⁻ Centers in Diamond at Room Temperature. *Phys. Rev. B* **2023**, *107*, L140101. [CrossRef]
- 50. Harris, I.B.W.; Englund, D. Coherence of Group-IV Color Centers. Phys. Rev. B 2024, 109, 085414. [CrossRef]
- 51. Yang, G.; Fragner, A.; Koolstra, G.; Ocola, L.; Czaplewski, D.A.; Schoelkopf, R.J.; Schuster, D.I. Coupling an Ensemble of Electrons on Superfluid Helium to a Superconducting Circuit. *Phys. Rev. X* **2016**, *6*, 011031. [CrossRef]
- 52. Koolstra, G.; Glen, E.; Beysengulov, N.; Byeon, H.; Castoria, K.; Sammon, M.; Dizdar, B.; Wang, C.; Schuster, D.; Lyon, S.; et al. High-impedance resonators for strong coupling to an electron on helium. *Phys. Rev. Appl.* **2025**, 23, 024001. [CrossRef]
- 53. Belianchikov, M.; Morais, N.; Konstantinov, D. Image-Charge Detection of Electrons on Helium in an on-Chip Trapping Device. *Phys. Rev. Appl.* **2025**, *23*, 054026. [CrossRef]
- 54. Koolstra, G.; Yang, G.; Schuster, D.I. Coupling a Single Electron on Superfluid Helium to a Superconducting Resonator. *Nat. Commun.* **2019**, *10*, 5323. [CrossRef] [PubMed]
- 55. Castoria, K.E.; Beysengulov, N.R.; Koolstra, G.; Byeon, H.; Glen, E.O.; Sammon, M.; Lyon, S.A.; Pollanen, J.; Rees, D.G. Sensing and Control of Single Trapped Electrons Above 1 Kelvin. *arXiv* 2024. [CrossRef]
- 56. Platzman, P.M.; Dykman, M.I. Quantum Computing with Electrons Floating on Liquid Helium. *Science* **1999**, 284, 1967–1969. [CrossRef]
- 57. Dykman, M.I.; Platzman, P.M.; Seddighrad, P. Qubits with Electrons on Liquid Helium. Phys. Rev. B 2003, 67, 155402. [CrossRef]
- 58. Schuster, D.I.; Fragner, A.; Dykman, M.I.; Lyon, S.A.; Schoelkopf, R.J. Proposal for Manipulating and Detecting Spin and Orbital States of Trapped Electrons on Helium Using Cavity Quantum Electrodynamics. *Phys. Rev. Lett.* **2010**, *105*, 040503. [CrossRef]
- 59. Pollanen, J.; Beysengulov, N.; Rees, D. Qubit Hardware for Electrons on Helium. US10892398B2, 12 January 2021.
- 60. Beysengulov, N.R.; Pollanen, J.; Schøyen, Ø.S.; Bilek, S.D.; Flaten, J.B.; Leinonen, O.; Kristiansen, H.E.; Stewart, Z.J.; Weidman, J.D.; Wilson, A.K.; et al. Coulomb Interaction-Driven Entanglement of Electrons on Helium. *arXiv* 2023, arXiv:2310.04927. [CrossRef]
- 61. Nielsen, M.A.; Chuang, I.L. *Quantum Computation and Quantum Information: 10th Anniversary Edition*, 1st ed.; Cambridge University Press: Cambridge, UK; New York, NY, USA, 2011.
- 62. Cole, M.W. Electronic Surface States of Liquid-Helium. Rev. Mod. Phys. 1974, 46, 451–464. [CrossRef]
- 63. Grimes, C.C.; Brown, T.R.; Burns, M.L.; Zipfel, C.L. Spectroscopy of Electrons in Image-Potential-Induced Surface States Outside Liquid Helium. *Phys. Rev. B* **1976**, *13*, 140. [CrossRef]
- 64. Pekar, S.I. Theory of Color Centers. Zh. Eksper. Teor. Fiz. 1950, 20, 510.
- 65. Huang, K.; Rhys, A. Theory of Light Absorption and Non-Radiative Transitions in f-Centres. *Proc. R. Soc. Lond. Ser. A Math. Phys. Sci.* **1950**, 204, 406–423. [CrossRef]
- 66. Markham, J.J. Interaction of Normal Modes with Electron Traps. Rev. Mod. Phys. 1959, 31, 956–989. [CrossRef]
- 67. Krivoglaz, M.A.; Pekar, S.I. Spectra of Impurity Light Absorption and Luminescence in Dielectrics. *Proc. Inst. Phys. Ukr. Acad. Sci.* **1953**, *4*, 37–70.

Entropy 2025, 27, 787 18 of 18

68. Wudarski, F.; Zhang, Y.; Dykman, M.I. Nonergodic Measurements of Qubit Frequency Noise. *Phys. Rev. Lett.* **2023**, *131*, 230201. [CrossRef]

- 69. Ritter, J.T.; Markman, J.J. Theory of Electron-Phonon Interaction and Defect-Center Optical Spectra. *Phys. Rev.* **1969**, 185, 1201–1213. [CrossRef]
- 70. Baldacchini, G.; Pan, D.S.; Lüty, F. Radiative and Nonradiative Processes of *F* and *F'* Centers in NaBr and NaI. *Phys. Rev. B* **1981**, 24, 2174–2186. [CrossRef]
- 71. Lamelas, A.; Amaral, V.S. Extracting Phonon Coupling Parameters from Multi Color Center Photoluminescence. *J. Opt.* **2024**, 26, 095404. [CrossRef]
- 72. Tabbert, B.; Günther, H.; zu Putlitz, G. Optical Investigation of Impurities in superfluid⁴He. *J. Low Temp. Phys.* **1997**, *109*, 653–707. [CrossRef]
- 73. Fowler, W.B.; Dexter, D.L. Electronic Bubble States in Liquid Helium. Phys. Rev. 1968, 176, 337–343. [CrossRef]

Disclaimer/Publisher's Note: The statements, opinions and data contained in all publications are solely those of the individual author(s) and contributor(s) and not of MDPI and/or the editor(s). MDPI and/or the editor(s) disclaim responsibility for any injury to people or property resulting from any ideas, methods, instructions or products referred to in the content.